Journal of Hepatocellular Carcinoma

Dovepress
open access to scientific and medical research

Open Access Full Text Article

ORIGINAL RESEARCH

The Enhanced Role of Eosinophils in Radiomics-Based Diagnosis of Microvascular Invasion and Its Association with the Immune Microenvironment in Hepatocellular Carcinoma

Dong Liu[1,*], Jianmin Wu[2,*], Han Wang[3], Hui Dong[3], Lei Chen[4], Ningyang Jia[1]

[1]Department of Radiology, The Third Affiliated Hospital of Naval Medical University, Shanghai, 200433, People's Republic of China; [2]Shanghai Key Laboratory of Metabolic Remodeling and Health, Institute of Metabolism and Integrative Biology, Fudan University, Shanghai, 200438, People's Republic of China; [3]Department of Pathology, The Third Affiliated Hospital of Naval Medical University, Shanghai, 200433, People's Republic of China; [4]The International Cooperation Laboratory on Signal Transduction, Eastern Hepatobiliary Surgery Hospital, Naval Medical University, Shanghai, 201805, People's Republic of China

*These authors contributed equally to this work

Correspondence: Ningyang Jia; Lei Chen, Email ningyangjia@163.com; chenlei@smmu.edu.cn

Objective: To investigate the role of eosinophil counts (EC) in microvascular invasion (MVI) for enhancing the radiomics based diagnostic model. Additionally, its correlation with early recurrence and tumor immune microenvironment was explored.

Methods: Propensity score matching was employed to evaluate on 462 cases whether EC was an independent risk factor for MVI. Subgroup analyses examined EC's effect on MVI across varying hypersplenism degrees. Univariate-multivariate logistic regression identified MVI's independent factors to develop a diagnostic model. Univariate-multivariate COX regression determined early recurrence factors. Co-detection by indexing (CODEX) constructed the immune score (IS), and Spearman correlation analyzed its association with peripheral immunity.

Results: EC was an independent risk factor for MVI (p=0.038, OR=1.304 (95% CI: 1.014–1.677)), and its effect on MVI disappeared with the severity of hypersplenism. The diagnostic model with EC was significantly improved (AUC=0.787 (95% CI: 0.737–0.836) vs AUC=0.748(95% CI: 0.694–0.802, p=0.005)). MVI was an independent risk factor for early recurrence (p<0.001, HR = 2.254 (95% CI: 1.557–3.263)). IS was negatively correlated with lymphocyte counts (R=−0.311, p=0.022), and positively correlated with EC (R=0.301, p=0.027) and RS (R = 0.315, p = 0.018).

Conclusion: EC was an independent risk factor for MVI and was related to the tumor immune microenvironment. EC should be included in the diagnosis of MVI to improve diagnostic efficiency.

Keywords: hepatocellular carcinoma, eosinophils, radiomics

Introduction

Liver cancer ranks fifth among men and seventh among women among the top ten major cancer types in the United States based on the number of deaths in 2024.[1] Hepatocellular carcinoma (HCC) commonly exhibits postoperative recurrence, with a five-year recurrence rate reaching up to 70%.[2] Microvascular invasion (MVI), a critical pathological feature of HCC, has been established as a factor associated with recurrence and prognosis in prior studies.[3,4] While numerous studies have focused on the prediction and diagnosis of MVI through radiomics, they typically rely on clinical laboratory tests and imaging characteristics, often neglecting the role of peripheral immune cells.[5,6]

Eosinophils have been found to promote tumor angiogenesis and normalization, and regulate the immune composition of the tumor immune microenvironment (TIME).[7] The trafficking of immune cells in the TIME and peripheral blood allows the peripheral eosinophils to reflect the eosinophils within the tumor, as the eosinophils within the TIME is

Received: 8 August 2024
Accepted: 14 September 2024
Published: 25 September 2024

© 2024 Liu et al. This work is published and licensed by Dove Medical Press Limited. The full terms of this license are available at https://www.dovepress.com/terms.php and incorporate the Creative Commons Attribution – Non Commercial (unported, v3.0) License (http://creativecommons.org/licenses/by-nc/3.0/). By accessing the work you hereby accept the Terms. Non-commercial uses of the work are permitted without any further permission from Dove Medical Press Limited, provided the work is properly attributed. For permission for commercial use of this work, please see paragraphs 4.2 and 5 of our Terms (https://www.dovepress.com/terms.php).

scarce.[8] In this study, we utilized the propensity score matching (PSM) method to investigate whether eosinophil counts (EC) serve as an independent risk factor for MVI. We analyzed the changes in the role of EC in patients with varying degrees of hypersplenism within subgroups. Additionally, we examined whether a diagnostic model incorporating EC outperforms the traditional clinical-radiomics model. We assessed the correlations among EC, hypersplenism, MVI, and early recurrence, employing Co-detection by indexing (CODEX) technology to evaluate the TIME and explore the relationship between peripheral immunity and the TIME.

Materials and Methods

Study Population

The single-center, retrospective study was approved by the Ethical Committee of Eastern Hepatobiliary Surgery Hospital (EHBHKY2018-1–001), and each CODEX participant provided written informed consent, as was our previous study,[9] and it was conducted in adherence to the Declaration of Helsinki. Patient confidentiality was maintained by removing all identifying details from the data. Consecutive patients who underwent surgical resection for HCC at our hospital from January 2016 to April 2018 were enrolled, excluding those who met the following criteria: (1) incomplete medical records, especially lacking preoperative MRI or pathological findings; (2) MRI that could not be analyzed due to motion or metal artifacts; (3) prior receipt of antitumor therapy before surgery. Finally, a total of 462 patients were ultimately included and randomly divided into a training set and a validation set at a ratio of 7:3. 56 patients used CODEX to assess the TIME, and the experimental procedure was the same as our previous study.[9] However, in this study, we evaluated 36 molecules, which was more than the previous 17 molecules. For cases of multiple HCCs, the tumor with the largest diameter was analyzed in the radiomics process.

Baseline clinical characteristics were collected from medical records, including age, gender, alpha-fetoprotein (AFP), alanine aminotransferase (ALT), aspartate aminotransferase (AST), total bilirubin (TBIL), carcinoembryonic antigen (CEA), carbohydrate antigen 19–9 (CA19-9), hypersplenism (HS), and peripheral immune cell counts (neutrophils, lymphocytes, monocytes, eosinophils, basophils). Radiological and pathological features, such as tumor size, number (multiple), Edmondson-Steiner grade (III–IV), cirrhosis, morphology (irregular), and presence of necrosis or hemorrhage, were also collected. The research flow chart was shown in Figure 1.

Propensity Score Matching and Subgroup Analysis

Propensity score matching (PSM) was employed to balance the baseline characteristics of EC. The enrolled patients were divided into EC-0 and EC-1 groups according to the mean value of eosinophil counts. A random seed was set to "123456". Independent variables with $p < 0.05$ were used to construct the propensity score. The nearest neighbor method was utilized for matching, with a caliper value set at 0.1. The target group and the control group were matched in a 1:1 ratio.

Given that hypersplenism significantly affects peripheral blood cell counts, the enrolled patients were divided into three groups based on the degree of hypersplenism:[10] (1) Absent: patients without hypersplenism, showing normal peripheral blood counts; (2) Mild: patients with a platelet count less than 100×10^9/L; (3) Severe: patients with a platelet count less than 50×10^9/L. The relationship between EC and MVI was then investigated within these three groups.

Radiomics Feature Extraction and Selection

MR images were acquired using a GE Optima MR360 1.5T scanner (Optima MR360, GE Healthcare, USA) equipped with an 8-channel abdominal coil. The imaging protocol included plain T1WI, FS-T2WI, and DWI (b=0, 600 s/mm^2), with plain FS-T2WI used for radiomics feature extraction.

Image segmentation was performed using the open-source software ITK-SNAP (v. 3.8.0, http://www.itksnap.org). A radiologist (L.D). with 5 years of experience in liver MRI manually outlined the volume of interest (VOI) for each patient layer by layer to delineate the entire tumor boundary in the FS-T2WI sequence. The segmentation results were validated for 30 randomly selected patients using the intraclass correlation coefficient (ICC) by another radiologist with over 10 years of experience in liver MRI(J.NY). Only features with ICC $\geq$ 0.8 were retained.

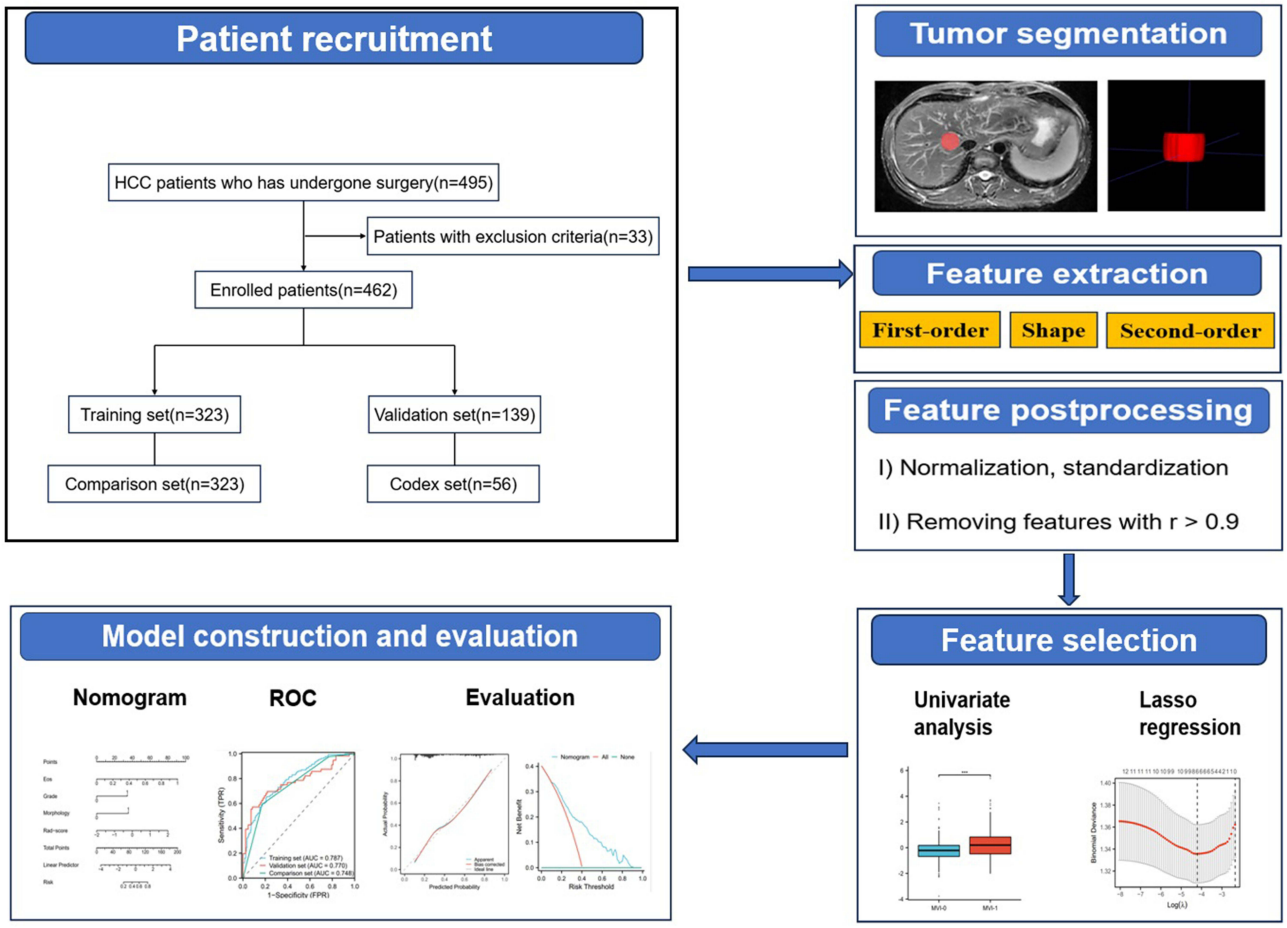

Figure 1 The flowchart of this study.

All segmented VOIs were loaded into Python, and feature extraction was performed using the pyradiomics package, adhering to the Image Biomarker Standardization Initiative (IBSI). The radiomics features were categorized into three primary types: (a) first-order statistics, (b) shape features, and (c) second-order statistics, including the gray level co-occurrence matrix (GLCM), gray level run length matrix (GLRLM), gray level size zone matrix (GLSZM), gray level dependence matrix (GLDM), and neighborhood gray tone difference matrix (NGTDM).

To eliminate differences in data dimensionality, radiomics features were standardized using z-score normalization. Features with a Spearman correlation >0.9 were pruned,[11] retaining only one of each correlated pair. Stable features were analyzed using single-factor tests (*T*-test or Mann–Whitney *U*-test), and significant features for MVI ($p < 0.05$) were selected. Least absolute shrinkage and selection operator (LASSO) regression was then employed to identify key radiomics features for MVI diagnosis and to formulate an equation for the radiomic-score (RS). A five-fold cross-validation approach was used to determine the optimal value of the penalization parameter lambda (λ).

Model Construction and Validation

Univariate logistic analysis was conducted on clinical, radiological (including RS), and pathological features. Variables with $p < 0.05$ were included in the multivariate logistic analysis to identify independent diagnostic factors for MVI. A model was then established, visualized using a nomogram, and evaluated through calibration curve and decision curve analysis (DCA). To compare models, a comparison set was created by excluding peripheral immunity and employing the same method. The areas under the curves (AUCs) of the training set and the comparison set were compared using the DeLong test.

Histopathology

The pathology department determined the MVI status, which was documented in the medical records. MVI was defined as the microscopic presence of tumor thrombi within the small vessels adjacent to the tumor, potentially involving hepatic veins, portal veins, or significant capsular vessels near the surrounding liver tissue.

CODEX Set

The CODEX technology, a multi-faceted tissue visualization system, was pioneered by Garry P. Nolan and his team at Akoya Biosciences.[12] Our investigation employed formalin-stabilized, paraffin-infiltrated (FFPE) tissues along with tissue microarrays (TMAs) sourced from HCC patients treated at our hospital. All participants provided their written, informed assent prior to inclusion, as was our previous study.[9]

36 immune-related biomarkers were selected for CODEX staining, including DAPI, FOXP3, p-mTOR, Twist1, PD-L1, p53, p-AMPK, PD1, c-Myc, Caspase-3, CD163, CD45, HIF1a, CD45RO, CD107A, aSMA, CD21, CD68, Hepar1, CD8, CD3, Glypican3, Keratin, CD4, p-S6, KI67, CD11C, Vimentin, E-Cadherin, HLA-DR, CD44, HistoneH3, CD20, Podoplanin, CD31, Pan-CK. Univariate analysis and LASSO regression were used to construct an immune score (IS) according to MVI status.

Follow-up

Patients were routinely monitored for recurrence every 3–6 months following surgery. Early recurrence (ER) was defined as a confirmed diagnosis of focal recurrence detected through enhanced MRI or CT examination within two years of the surgical procedure. Patients who lacked imaging data were excluded from the follow-up analysis.

Statistical Analysis

Comprehensive statistical evaluations were conducted using SPSS (version 27.0, Chicago, IL, USA) and R software (version 4.3.2, Vienna, Austria). Continuous variables were represented as mean ± SD, while categorical variables were presented as percentages. Depending on the data distribution, continuous variables were analyzed using either a two-sample *T*-test or a Mann–Whitney *U*-test. For categorical variables, the chi-squared test or Fisher's exact test was applied. Log rank test and multivariate Cox regression analysis were used to explore the factors influencing ER. The threshold for statistical significance was set at a two-sided *p*-value of less than 0.05.

Results

Patient Characteristics

Among the 462 patients included, 186 were MVI-positive and 276 were MVI-negative. Of these, 385 were male, and 77 were female. The age distribution ranged from 25 to 86, with an average of 56.09 ± 10.42 years. After successful PSM of 276 cases, EC were compared between the MVI-negative and MVI-positive groups through univariate analysis. The results indicated that EC was an independent risk factor for MVI ($p = 0.038$, OR = 1.304 (95% CI: 1.014–1.677)). Details before and after matching were shown in Table 1. Probability density before and after PSM was detailed in Figure 2a, and Absolute mean differences were detailed in Figure 2b. In the subgroup analysis of hypersplenism, it was found that in the subgroup without hypersplenism, EC was associated with MVI ($p = 0.048$, OR = 1.644 (95% CI: 1.014–1.677)). However, as hypersplenism worsened, the correlation between EC and MVI disappeared (Figure 3).

Model Construction and Comparison

Ultimately, 7 out of 1834 radiomics features were selected to construct the RS. The formula was as follows:

RS=−0.389–0.097*original_glcm_MaximumProbability
-0.041*original_gldm_LargeDependenceLowGrayLevelEmphasis
+0.080*original_glszm_SizeZoneNonUniformity
+0.026*original_ngtdm_Complexity
-0.148*original_shape_Elongation
-0.235*original_shape_Sphericity.

Table 1 The Results Before and After Propensity Score Matching (PSM)

Variable	Before PSM				After PSM			
	EC-0 (n = 298)	EC-1 (n = 164)	*p value*	SMD	EC-0 (n = 298)	EC-1 (n = 164)	*p value*	SMD
Age, mean ± SD	55.7 ± 10.3	56.9 ± 10.3	0.235	0.110	56.5 ± 10.1	56.3 ± 10.6	0.906	−0.014
Gender(male,%)	244 (80.0)	168 (88.4)	**0.015**	0.263	120 (82.2)	127 (87.0)	0.257	0.143
AFP, ng/mL	230.8 ± 399.3	239.0 ± 412.0	0.826	0.020	231.9 ± 400.1	257.5 ± 432.7	0.600	0.059
ALT, U/L	38.7 ± 59.4	39.1 ± 49.0	0.934	0.009	36.9 ± 33.9	42.4 ± 54.8	0.303	0.100
AST, U/L	34.0 ± 47.4	35.7 ± 48.7	0.711	0.034	31.6 ± 20.1	39.3 ± 54.6	0.114	0.140
TBIL, μmol/L	16.6 ± 7.5	14.7 ± 7.0	**0.005**	−0.275	14.8 ± 6.0	14.9 ± 7.3	0.890	0.015
CEA, ng/mL	2.9 ± 2.2	3.3 ± 4.4	0.292	0.072	3.0 ± 2.6	3.4 ± 4.9	0.442	0.072
CA199, U/mL	25.3 ± 60.6	22.5 ± 22.6	0.538	−0.126	22.0 ± 20.1	23.3 ± 24.4	0.639	0.050
Neut, 10^9/L	2.7 ± 1.2	3.0 ± 1.0	**0.006**	0.286	2.8 ± 1.1	2.9 ± 1.0	0.331	0.115
Lymph, 10^9/L	1.5 ± 0.6	1.7 ± 0.6	**<0.001**	0.480	1.6 ± 0.6	1.6 ± 0.5	0.505	0.087
Mono, 10^9/L	0.3 ± 0.1	0.4 ± 0.1	**<0.001**	0.546	0.4 ± 0.1	0.4 ± 0.1	0.544	0.078
Baso, 10^9/L	0.0 ± 0.0	0.0 ± 0.0	**<0.001**	0.579	0.0 ± 0.0	0.0 ± 0.0	0.902	−0.013
HS(present,%)	165 (54.1)	65 (34.2)	**<0.001**	−0.419	63 (43.2)	58 (39.7)	0.553	−0.070

Notes: HS hypersplenism, the p value with statistical significance was marked in bold.

Through multivariate logistic regression, four independent diagnostic factors of MVI were identified: EC ($p = 0.010$, OR = 1.526 (95% CI: 1.108–2.101)), grade ($p < 0.001$, OR = 4.927 (95% CI: 1.953–12.429)), morphology ($p < 0.001$, OR = 5.195 (95% CI: 3.062–8.813)), and RS ($p = 0.006$, OR = 2.533 (95% CI: 1.297–4.945)). Based on these factors,

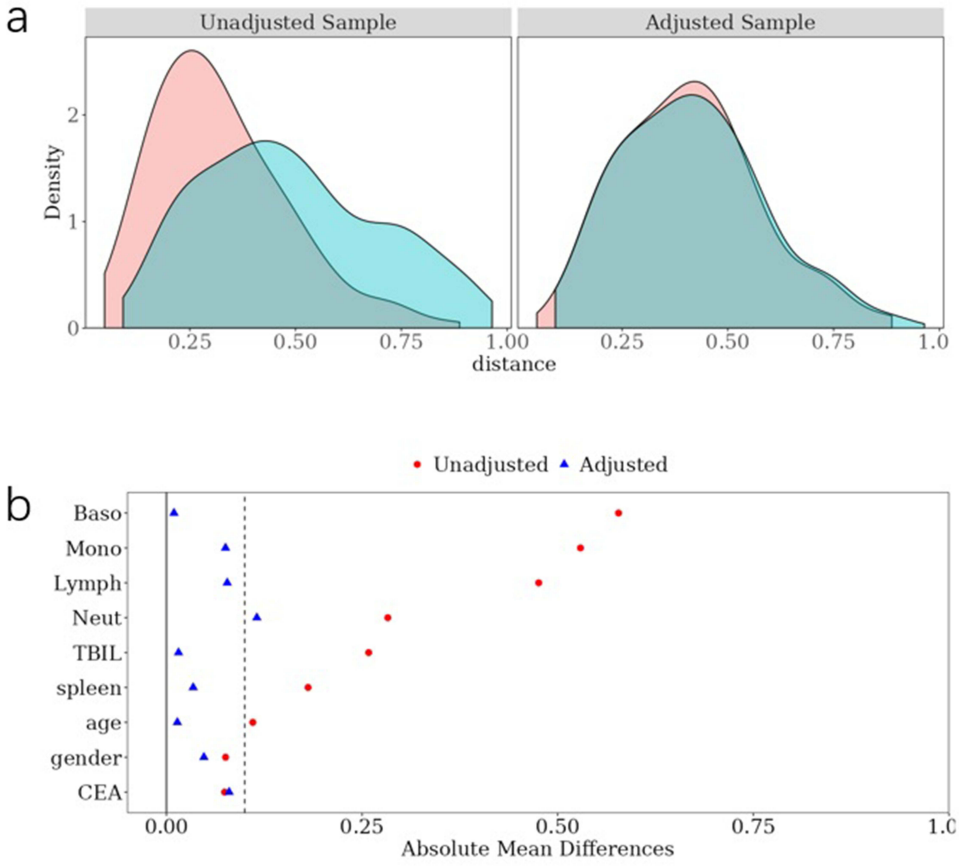

Figure 2 Schematic Diagram of Propensity Score Matching. (**a**) Probability density analysis before and after matching. (**b**) Absolute Mean Differences analysis before and after matching.

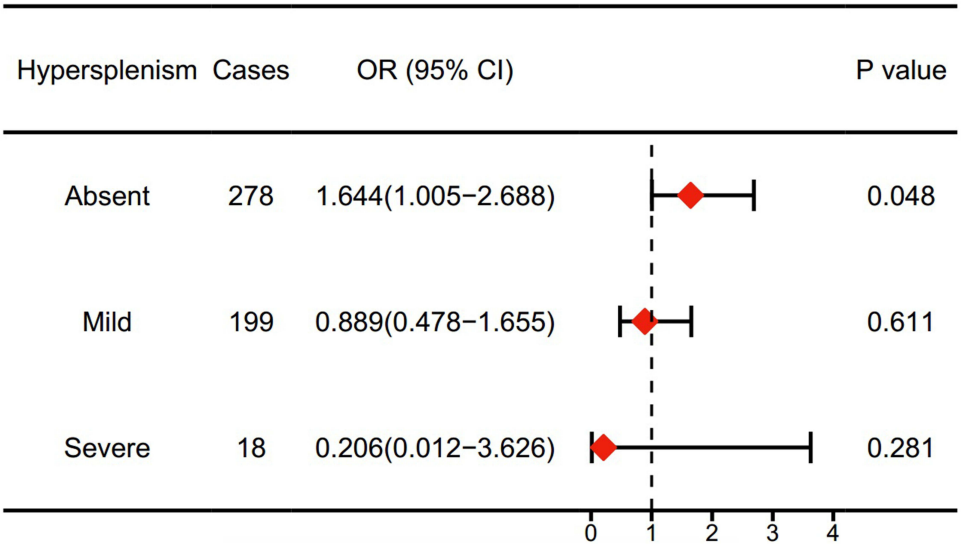

Figure 3 Forest plot. The effect of eosinophil counts on microvascular invasion disappeared with the severity of hypersplenism.

a nomogram was constructed (Figure 4a). The calibration curve (Figure 4b) demonstrated good consistency between the diagnostic probability of MVI predicted by the nomogram and the actual probability. The DCA curve (Figure 4c) indicated that the net benefit of the nomogram was optimal when the threshold probability was greater than 0.1. Variables selection was shown in Tables 2–4.

The model exhibited robust diagnostic performance in identifying MVI in both the training set ($p < 0.001$, AUC = 0.787 (95% CI: 0.737–0.836)) and the validation set ($p < 0.001$, AUC = 0.770 (95% CI: 0.685–0.854)). After excluding EC, the performance of the comparison set ($p < 0.001$, AUC = 0.748 (95% CI: 0.694–0.802)) was inferior to the training set, and the DeLong test revealed a significant statistical difference in AUC between the two sets ($z = -2.82$, $p = 0.005$), further emphasizing the necessity of including EC in the model (Figure 4d). The performance of the training set, validation set, and comparison set was shown in Table 5.

Predictors of Early Recurrence

A total of 167 patients had clear follow-up information, with 115 cases experiencing early recurrence and 52 not. The duration of early recurrence ranged from 33 to 707 days. The Log rank test and multivariate Cox regression analysis showed that the presence of hypersplenism ($p = 0.086$, HR = 1.379 (95% CI: 0.955–1.990)) and EC ($p = 0.953$, HR = 0.941 (95% CI: 0.122–7.234)) had no statistically significant impact on the time of early recurrence. However, the occurrence of MVI had a statistically significant impact on the time of early recurrence and was identified as an independent risk factor ($p < 0.001$, HR = 2.254 (95% CI: 1.557–3.263)).

Relationship Between EC and Immune Microenvironment

IS was constructed according to the following formula: IS = −0.568 −5.177*DAPI + 3.615*caspase - 3-5.203*aSMA. We explored the correlation between hypersplenism, peripheral immune cell counts (neutrophils, lymphocytes, monocytes, eosinophils, basophils), and IS in HCC. It was found that lymphocyte counts negatively correlated with IS (R = −0.311, $p = 0.022$), while EC positively correlated with IS (R = 0.301, $p = 0.027$). Other immune cell counts and hypersplenism showed no significant correlation with IS (Figure 5a). Additionally, a positive correlation between IS and *RS* was observed (R = 0.315, p = 0.018) (Figure 5b). Typical cases were shown in Figure 6, with Figure 6a–c showed FS-T2WI MRI, CODEX and MVI-negative pathological images of a HCC patient without MVI, and Figure 6d–f showed the compared images of a patient with MVI.

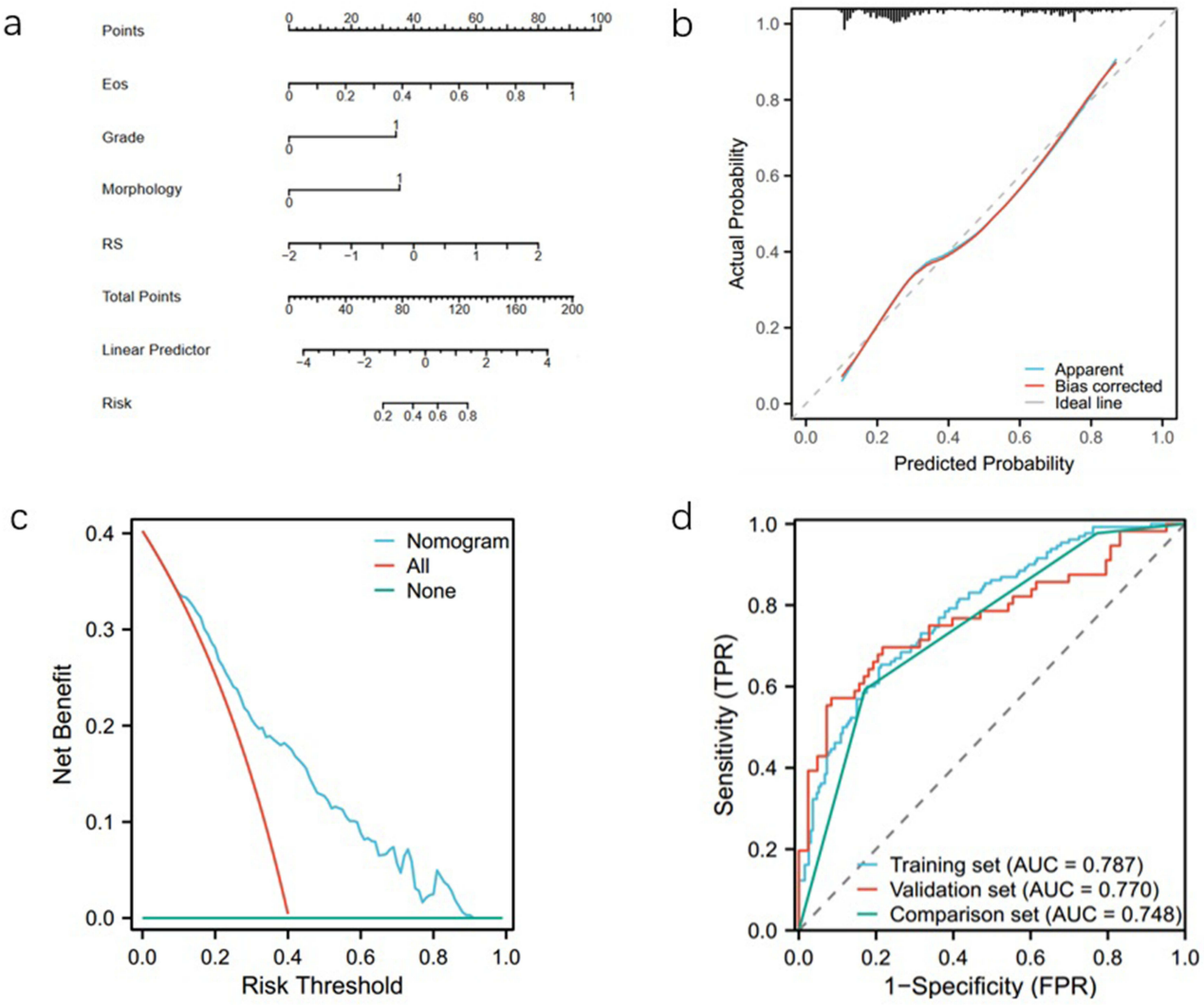

Figure 4 (**a**) The nomogram for diagnosis of MVI. (**b**) The calibration curve. (**c**) The decision curve analysis. (**d**) The receiver operating characteristic curves for the training set, validation set, and comparison set.

Discussion

In our study, utilizing PSM, subgroup analysis revealed that EC was an independent risk factor for MVI. Hypersplenism decreased EC and lessened the effect of eosinophils on MVI. We then developed a radiomics model incorporating EC for diagnosing MVI and found significant improvements compared to the model without EC. While MVI significantly influenced the time to early recurrence, EC and hypersplenism did not. Lastly, we examined the correlation between peripheral immunity and the tumor immune microenvironment, finding that IS was negatively correlated with lymphocyte counts, and positively correlated with EC and RS.

The use of radiomics in diagnosing MVI in HCC has been a major research focus. Among the various risk factors for MVI, tumor size,[13] margin,[14] AFP level,[15] and enhancement pattern[6,14] have been identified as independent predictors. However, the potential role of EC has been scarcely investigated. The link between eosinophils and tumors, first reported a century ago,[16] has evolved to understand eosinophils as immune cells with variable pro- or anti-tumor properties depending on the tumor microenvironment.[17] Eosinophils acted as a protective factor in pancreatic cancer,[18] but as a risk factor in malignant lung nodules[19] and cervical cancer.[20] Early in tumor development, eosinophils were few and exhibited anti-tumor properties, aiding in immune surveillance and Th1 responses. However, as the disease advanced and eosinophil counts rose, activated eosinophils directed naïve CD4+ T cells towards a Th2 phenotype, creating

Table 2 Clinical Features in the Training and Validation Sets

Characteristics	Training Set(n=323)			Validation Set(n=139)			*p* value
	MVI-0(n=193)	MVI-1(n=130)	*p* value	MVI-0(n=83)	MVI-1(n=56)	*p* value	
Age, mean ± SD	55.3±10.5	55.9±10.6	0.628	57.6±10.6	57.0±9.3	0.738	0.085
Gender (male, %)	159(82.4)	104(80.0)	0.662	71(85.5)	51(91.1)	0.432	0.103
AFP, ng/mL	183.7±356.5	275.8±426.2	**0.045**	255.6±444.7	310.6±443.2	0.478	0.167
ALT, U/L	38.3±41.1	39.2±41.9	0.843	47.4±106.5	32.2±18.3	0.297	0.640
AST, U/L	31.1±23.8	38.5±47.8	0.111	42.0±91.6	31.6±17.8	0.413	0.446
TBIL, μmol/L	15.7±7.3	15.2±7.2	0.550	15.3±4.9	18.0±10.1	0.070	0.238
CEA, ng/mL	3.3±4.4	3.2±2.7	0.812	2.7±1.5	2.9±1.8	0.575	0.204
CA199, U/mL	22.2±23.1	21.7±20.2	0.831	25.2±26.1	21.7±19.5	0.410	0.431
Neut, 10^9/L	2.9±1.2	2.9±1.2	0.916	2.8±1.1	2.6±0.7	0.102	0.287
Lymph, 10^9/L	1.6±0.6	1.5±0.5	0.074	1.6±0.6	1.6±0.7	0.757	0.183
Mono, 10^9/L	0.3±0.1	0.3±0.1	0.806	0.4±0.1	0.3±0.1	0.704	0.995
Eos, 10^9/L	0.1±0.1	0.1±0.1	**0.009**	0.1±0.1	0.2±0.2	0.005	0.195
Baso, 10^9/L	0.0±0.0	0.0±0.0	0.796	0.0±0.0	0.0±0.0	0.111	0.387
HS(present,%)	80(41.5)	63(48.5)	0.253	33(39.8)	28(50.0)	0.296	1.000

Notes: HS hypersplenism, the p value with statistical significance was marked in bold.

Table 3 Radiological and Pathological Features in the Training and Validation Sets

Radiological and Pathological Features	Training Set(n=323)			Validation Set(n=139)			*p* value
	MVI-0 (n=193)	MVI-1 (n=130)	*p* value	MVI-0 (n=83)	MVI-1 (n=56)	*p* value	
Size, mean ± SD	3.3±1.8	3.7±2.7	0.102	3.0±1.6	3.6±2.4	0.078	0.355
Number (multiple, %)	24(12.4)	36(27.7)	**<0.001**	7(0.1)	13(23.2)	**0.025**	0.348
Grade(III~IV, %)	142(73.6)	124(95.4)	**<0.001**	57(68.7)	51(91.1)	**0.002**	0.247
Cirrhosis(present, %)	103(53.4)	79(60.8)	0.209	36(43.4)	29(51.8)	0.387	0.067
Morphology(irregular, %)	40(20.7)	80(61.5)	**<0.001**	28(33.7)	36(64.3)	**<0.001**	0.079
Necrosis or hemorrhage(present, %)	20(10.4)	16(12.3)	0.593	15(18.1)	9(16.1)	0.822	0.096
RS, mean ± SD	−0.5±0.4	−0.3±0.5	**<0.001**	−0.5±0.3	−0.3±0.5	**0.003**	0.846

Notes: The p value with statistical significance was marked in bold.

Table 4 Results of Univariate and Multivariate Logistic Regression Analyses

Variables	Univariate Analysis		Multivariate Analysis	
	OR(95% CI)	*p* value	OR(95% CI)	*p* value
AFP, ng/mL	1.443(1.141–1.825)	0.002	1.303(0.991–1.713)	0.058
Eos, 10^9/L	1.326(1.009–1.743)	0.043	1.495(1.065–2.098)	0.020
Number (multiple, %)	1.456(1.171–1.810)	<0.001	1.154(0.893–1.491)	0.274
Grade(III~IV, %)	2.121(1.525–2.949)	<0.001	1.772(1.250–2.513)	0.001
Morphology(irregular, %)	2.419(1.900–3.081)	<0.001	2.236(1.721–2.907)	<0.001
RS, mean ± SD	1.704(1.314–2.210)	<0.001	1.356(1.016–1.808)	0.038

Table 5 Performance of Diagnostic Models on Different Sets

Model	AUC(95% CI)	Accuracy	Sensitivity	Specificity
Training set	0.787(0.737–0.836)	0.822	0.654	0.788
Validation set	0.770(0.685–0.854)	0.787	0.571	0.916
Comparison Set	0.748(0.694–0.802)	0.825	0.592	0.829

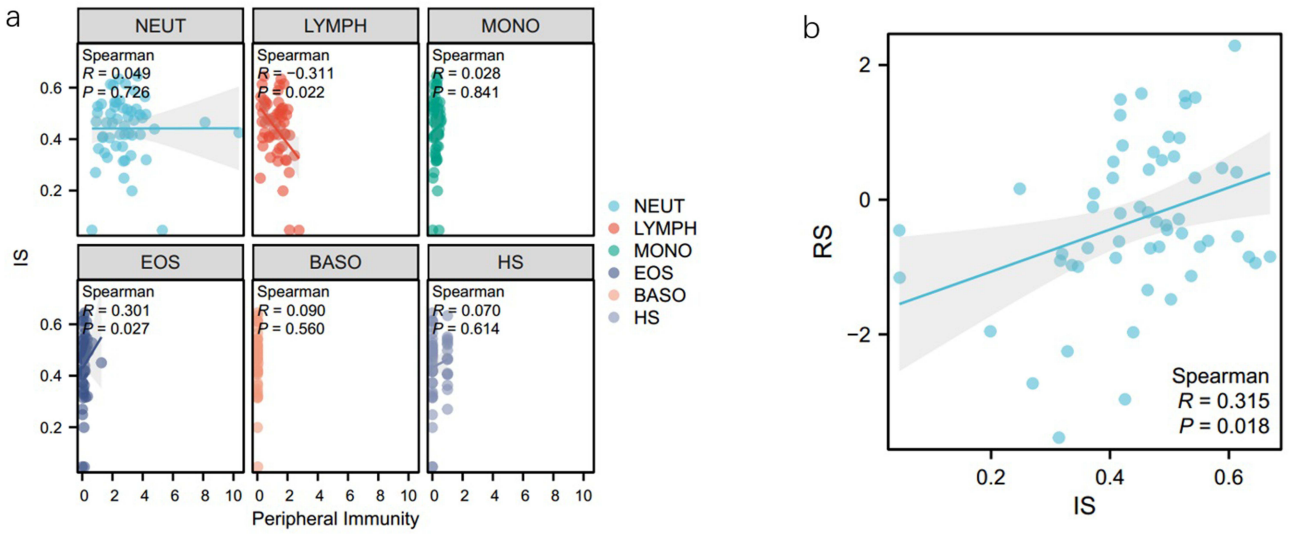

Figure 5 (**a**) The scatter plot of correlation between peripheral immunity and immune score (IS). (**b**) The scatter plot of correlation between radiomics score (RS) and IS.

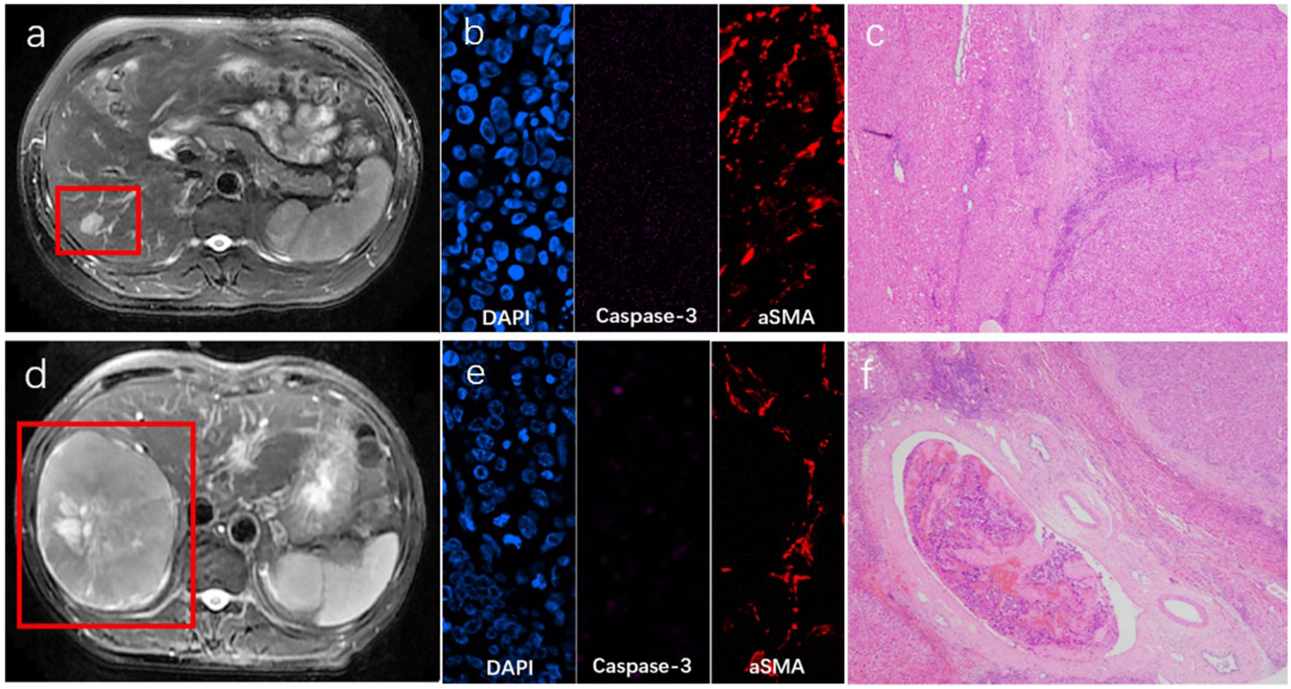

Figure 6 (**a–c**) FS-T2WI MRI, CODEX and MVI-negative pathological images of a HCC patient without MVI. (**d–f**) FS-T2WI MRI, CODEX and MVI-positive pathological images of a HCC patient with MVI.
Notes: The red square outlines in (**a** and **d**) each identified their respective HCC lesions; The pathological images were taken with a 4x objective lens.

a feedback loop that increased eosinopoiesis and suppressed Th1 responses. This Th2 dominance promoted an environment that supported tumor growth.[21]

In the context of HCC, EC showed a negative correlation with prognosis,[8] but their connection with MVI was less explored. Our study identified EC as an independent risk factor for MVI, potentially due to the degranulation of activated eosinophils, which release various pro-angiogenic factors. Upon IL-5 stimulation, eosinophils secrete vascular endothelial growth factor A (VEGFA), significantly promoting angiogenesis.[7] Additionally, eosinophils helped normalize tumor

vessels, an effect increased by the co-transfer of T cells, which replaced large dilated vessels with numerous small vessels.[22] Furthermore, Th2 polarization of eosinophils advanced tumor progression, increased tumor cell-blood vessel contact, and raised the likelihood of MVI, thereby highlighting eosinophils as a key risk factor for MVI in HCC.

Subgroup analysis showed that the impact of eosinophils on MVI decreased with the severity of hypersplenism. Cancer cells can regulate spleen immunity and influence HCC development. Spleen-resident or spleen-derived immune cells can release cytokines and directly alter the population of hepatic white blood cells after recruitment, creating a tumor-promoting immune microenvironment in the liver. The spleen played a central role in peripheral immunity, and when combined with spleen and/or blood immune parameters, it had a higher predictive value for late recurrence of HCC.[23] Subgroup analysis revealed that, in addition to complications from liver cirrhosis, the spleen's complex function in HCC also cushioned the effect of peripheral eosinophils on MVI.

This study found that EC, hypersplenism, and early recurrence were not significantly related, while MVI was an independent risk factor for early recurrence. Many previous studies[4,24,25] have identified MVI as a risk factor for recurrence and poor prognosis of HCC. In our study, we discovered that EC was an independent risk factor for MVI, but it did not affect the timing of early recurrence. Therefore, it is possible that eosinophils influence early recurrence time by affecting MVI. This hypothesis requires further research and verification.

Utilizing CODEX technology, we concurrently detected 36 immune-related biomarkers in HCC tumors. This comprehensive method enabled us to evaluate the immune microenvironment within the tumor and reduced the potential batch effect introduced by multiple immunohistochemical sections. Through LASSO regression analysis, we identified DAPI, Caspase-3, and aSMA as significant markers influencing MVI. Specifically, DAPI and Caspase-3 were identified as apoptosis markers, while aSMA was a serological marker for autoimmune hepatitis. Our constructed IS, based on MVI, showed an inverse correlation with lymphocyte counts and a positive correlation with EC, indicating that lymphocytes were protective factors for IS, whereas eosinophils were risk factors. Peripheral blood lymphocytes have been recognized as protective factors for HCC survival prognosis.[26,27] Our study found a significant association between IS and lymphocytes, while RS did not show a significant association with lymphocytes, suggesting that IS may be a more sensitive biomarker for the tumor microenvironment compared to RS. Furthermore, the positive correlation between IS and RS provides new insights into the biological significance of RS, indicating its potential to reflect the immune microenvironment of tumors before surgical intervention.

There are some limitations to our study. Firstly, blood cell counts fluctuate over time, so selecting only one snapshot of EC may be inaccurate. Secondly, eosinophils in peripheral blood are in an oxygen-rich, nutrient-rich, and pH-neutral environment, whereas eosinophils in the tumor microenvironment are in a metabolically challenging environment of hypoxia and low pH. Thus, peripheral blood eosinophils differ from tumor-infiltrating eosinophils,[28] necessitating further research on their role, especially in sequencing, which is currently lacking in most cases. Moreover, numerous studies have highlighted the importance of eosinophils in response to immunotherapy drugs. For instance, in non-small cell lung cancer[29–31] triple-negative breast cancer,[32] and HCC[33,34] treated with immunotherapy, patients with high baseline eosinophils show better responses and clinical outcomes. This highlights the complex role of eosinophils and calls for further research on their protective mechanism.

In summary, our study emphasized the importance of including EC in the development of a radiomics-based MVI diagnostic model. Additionally, this research explored the correlation between peripheral immune cells and the tumor immune microenvironment, revealing that while eosinophils were a risk factor, lymphocytes were a protective factor, warranting further investigation in the future.

Funding

This work was supported by The Project of Shanghai Municipal Commission of Health (2022LJ024).

Disclosure

The authors report no conflicts of interest in this work.

References

1. Siegel RL, Giaquinto AN, Jemal A. Cancer statistics, 2024. *Ca a Cancer J Clinicians*. 2024;74(1):12–49. doi:10.3322/caac.21820
2. Tampaki M, Papatheodoridis GV, Cholongitas E. Cholongitas E: intrahepatic recurrence of hepatocellular carcinoma after resection: an update. *Clin J Gastroenterol*. 2021;14(3):699–713. doi:10.1007/s12328-021-01394-7
3. Isik B, Gonultas F, Sahin T, Yilmaz S. Microvascular venous invasion in hepatocellular carcinoma: why do recurrences occur? *J Gastroint Can*. 2020;51(4):1133–1136. doi:10.1007/s12029-020-00487-9
4. Zhang Z-H, Jiang C, Qiang Z-Y, et al. Role of microvascular invasion in early recurrence of hepatocellular carcinoma after liver resection: a literature review. *Asian J Surg*. 2024;47(5):2138–2143. doi:10.1016/j.asjsur.2024.02.115
5. Lv K, Cao X, Du P, Fu J-Y, Geng D-Y, Zhang J. Radiomics for the detection of microvascular invasion in hepatocellular carcinoma. *World J Gastroenterol*. 2022;28(20):2176–2183. doi:10.3748/wjg.v28.i20.2176
6. Xia T, Zhou Z, Meng X, et al. Predicting microvascular invasion in hepatocellular carcinoma using CT-based radiomics model. *Radiology*. 2023;307(4):e222729. doi:10.1148/radiol.222729
7. De Visser KE, Joyce JA. The evolving tumor microenvironment: from cancer initiation to metastatic outgrowth. *Cancer Cell*. 2023;41(3):374–403. doi:10.1016/j.ccell.2023.02.016
8. Nixon AB, Schalper KA, Jacobs I, et al. Peripheral immune-based biomarkers in cancer immunotherapy: can we realize their predictive potential? *J Immuno Ther Can*. 2019;7(1):325–339. doi:10.1186/s40425-019-0799-2
9. Wu J, Liu W, Qiu X, et al. A noninvasive approach to evaluate tumor immune microenvironment and predict outcomes in hepatocellular carcinoma. *Phenomics*. 2023;3(6):549–564. doi:10.1007/s43657-023-00136-8
10. Chen X, Wang D, Dong R, et al. Effects of hypersplenism on the outcome of hepatectomy in hepatocellular carcinoma with hepatitis B virus related portal hypertension. *Front Surg*. 2023;10:1118693. doi:10.3389/fsurg.2023.1118693
11. Lin W-P, Xing K-L, J-C F, et al. Development and validation of a model including distinct vascular patterns to estimate survival in hepatocellular carcinoma. *JAMA Network Open*. 2021;4(9):e2125055. doi:10.1001/jamanetworkopen.2021.25055
12. Schürch CM, Bhate SS, Barlow GL, et al. Coordinated cellular neighborhoods orchestrate antitumoral immunity at the colorectal cancer invasive front. *Cell*. 2020;182(5):1341–1359. doi:10.1016/j.cell.2020.07.005
13. Hu H-T, Wang Z, Huang X-W, et al. Ultrasound-based radiomics score: a potential biomarker for the prediction of microvascular invasion in hepatocellular carcinoma. *Eur Radiol*. 2018;29(6):2890–2901. doi:10.1007/s00330-018-5797-0
14. Xu X, Zhang H-L, Liu Q-P, et al. Radiomic analysis of contrast-enhanced CT predicts microvascular invasion and outcome in hepatocellular carcinoma. *J Hepatol*. 2019;70(6):1133–1144. doi:10.1016/j.jhep.2019.02.023
15. Chong H, Yang L, Sheng R, et al. Multi-scale and multi-parametric radiomics of gadoxetate disodium–enhanced MRI predicts microvascular invasion and outcome in patients with solitary hepatocellular carcinoma ≤ 5 cm. *Eur Radiol*. 2021;31(7):4824–4838. doi:10.1007/s00330-020-07601-2
16. F F. The occurrence of eosinophilic leukocytes in tumours. *Arch Pathol Anat Physiol Klin Med*. 1900;161:1–18.
17. Simon SCS, Utikal J, Umansky V. Opposing roles of eosinophils in cancer. *Cancer Immunol Immunother*. 2018;68(5):823–833. doi:10.1007/s00262-018-2255-4
18. Ohkuma R, Kubota Y, Horiike A, et al. The prognostic impact of eosinophils and the eosinophil-to-lymphocyte ratio on survival outcomes in stage II resectable pancreatic cancer. *Pancreas*. 2021;50(2):167–175. doi:10.1097/MPA.0000000000001731
19. Xiu J, Wang X, Xu W, et al. Diagnostic value of peripheral blood eosinophils for benign and malignant pulmonary nodule. *Medicine*. 2023;102(44):e35936–e35941. doi:10.1097/MD.0000000000035936
20. Xie F, Liu LB, Shang WQ, et al. The infiltration and functional regulation of eosinophils induced by TSLP promote the proliferation of cervical cancer cell. *Cancer Lett*. 2015;364(2):106–117. doi:10.1016/j.canlet.2015.04.029
21. Sasan G, Nima R. Eosinophils in the tumor microenvironment: implications for cancer immunotherapy. *J Transl Med*. 2023;21(1):551–574. doi:10.1186/s12967-023-04418-7
22. Carretero R, Sektioglu IM, Garbi N, Salgado OC, Beckhove P, Hämmerling GJ. Eosinophils orchestrate cancer rejection by normalizing tumor vessels and enhancing infiltration of CD8+ T cells. *Nat Immunol*. 2015;16(6):609–617. doi:10.1038/ni.3159
23. Wei W, Li L, Kong G, Zheng Z, Ji F, Li Z. Spleen in hepatocellular carcinoma: more complexity and importance than we knew. *J Hepatol*. 2019;70(4):805–806. doi:10.1016/j.jhep.2018.11.022
24. Yang J, Qian J, Wu Z, et al. Exploring the factors affecting the occurrence of postoperative MVI and the prognosis of hepatocellular carcinoma patients treated with hepatectomy: a multicenter retrospective study. *Cancer Med*. 2024;1:1–14.
25. Li J, Su X, Xu X, et al. Preoperative prediction and risk assessment of microvascular invasion in hepatocellular carcinoma. *Crit Rev Oncol/Hematol*. 2023;190:104107. doi:10.1016/j.critrevonc.2023.104107
26. Hong YM, Yoon KT, Hwang TH, Cho M. Pretreatment peripheral neutrophils, lymphocytes and monocytes predict long-term survival in hepatocellular carcinoma. *BMC Cancer*. 2020;20(1):937–946. doi:10.1186/s12885-020-07105-8
27. Li JX, He ML, Qiu MQ, Yan LY, Long MY, Zhong JH. Prognostic value of a nomogram based on peripheral blood immune parameters in unresectable hepatocellular carcinoma after intensity-modulated radiotherapy. *BMC Gastroenterol*. 2022;22(1):510–521. doi:10.1186/s12876-022-02596-0
28. Mattei F, Andreone S, Marone G, et al. Eosinophils in the tumor microenvironment. *Adv Exp Med Biol*. 2020;1273:1–28.
29. Chu X, Zhao J, Zhou J, Zhou F, Jiang T, Jiang S. Association of baseline peripheral-blood eosinophil count with immune checkpoint inhibitor-related pneumonitis and clinical outcomes in patients with non-small cell lung cancer receiving immune checkpoint inhibitors. *Lung Cancer*. 2020;150:76. doi:10.1016/j.lungcan.2020.08.015
30. Okauchi S, Shiozawa T, Miyazaki K, Nishino K, Sasatani Y, Ohara G. Association between peripheral eosinophils and clinical outcome in non-small cell lung cancer patients treated with immune checkpoint inhibitors. *Polish Archiv Inter Med*. 2021;131(2):152–160. doi:10.20452/pamw.15776
31. Takeuchi E, Kondo K, Okano Y, et al. Pretreatment eosinophil counts as a predictive biomarker in non-small cell lung cancer patients treated with immune checkpoint inhibitors. *Thoracic Cancer*. 2023;14(30):3042–3050. doi:10.1111/1759-7714.15100

32. Ghebeh H, Elshenawy MA, AlSayed AD, Al-Tweigeri T. Peripheral blood eosinophil count is associated with response to chemoimmunotherapy in metastatic triple-negative breast cancer. *Immunotherapy*. 2022;14(4):189–199. doi:10.2217/imt-2021-0149
33. Toshida K, Itoh S, Yoshiya S, et al. Pretreatment eosinophil count predicts response to atezolizumab plus bevacizumab therapy in patients with hepatocellular carcinoma. *J Gastroenterol Hepatol*. 2023;39(3):576–586. doi:10.1111/jgh.16441
34. Orsi G, Tovoli F, Dadduzio V, et al. Prognostic role of blood eosinophil count in patients with sorafenib-treated hepatocellular carcinoma. *Targeted Oncol*. 2020;15(6):773–785. doi:10.1007/s11523-020-00757-3

Journal of Hepatocellular Carcinoma Dovepress

Publish your work in this journal

The Journal of Hepatocellular Carcinoma is an international, peer-reviewed, open access journal that offers a platform for the dissemination and study of clinical, translational and basic research findings in this rapidly developing field. Development in areas including, but not limited to, epidemiology, vaccination, hepatitis therapy, pathology and molecular tumor classification and prognostication are all considered for publication. The manuscript management system is completely online and includes a very quick and fair peer-review system, which is all easy to use. Visit http://www.dovepress.com/testimonials.php to read real quotes from published authors.

Submit your manuscript here: https://www.dovepress.com/journal-of-hepatocellular-carcinoma-journal